

Thermally excited 630.0 nm $O(^1D)$ emission in the cusp: A frequent high-altitude transient signature

Herbert C. Carlson,¹ Kjellmar Oksavik,² and Jøran I. Moen^{3,4}

Received 27 March 2013; revised 11 August 2013; accepted 13 August 2013; published 6 September 2013.

[1] We highlight why 630.0 nm auroral emissions excited by thermal electrons are expected to be significant in the cusp and are occurring more often than generally recognized. We note conditions when they are likely to occur and provide a simple formula to calculate the altitude discriminated (R/km) and line-of-sight integrated 630.0 nm intensity (kR). The formula is applied to incoherent scatter radar data near the cusp to produce 2-D maps of thermal red line aurora. We estimate when the thermally excited red aurora should be negligible or not, for given electron density (Ne), electron temperature (Te), and exospheric temperature (Tn) conditions. Sensitivity to Te dominates that to Tn and Ne. We test these formulas against radar and all-sky imaging photometer data for 2 days. The time/space agreement, as transient strong red arcs pass over the cusp, confirms detection of a thermal 630.0 nm aurora in ~400–450 km altitude, twice the height (4 times the area) conventionally assumed for 630.0 nm emissions. Among many potential uses for this technique is application to the long-standing question of the degree to which magnetic reconnection events contribute to the net magnetic flux entering the polar cap. We conclude that it is more often than now recognized and provide a tool and guidelines to facilitate improvement over present underestimates.

Citation: Carlson, H. C., K. Oksavik, and J. I. Moen (2013), Thermally excited 630.0 nm $O(^1D)$ emission in the cusp: A frequent high-altitude transient signature, *J. Geophys. Res. Space Physics*, 118, 5842–5852, doi:10.1002/jgra.50516.

1. Introduction

[2] It is common in auroral physics to use 630.0 nm optical emissions to characterize and trace phenomena important for understanding Earth's space environment, including its impact on practical systems operating in and through near-Earth space. For many purposes, the emission altitude is rather adequately estimated based on excitation by particle impact, dissociative recombination, and quenching. Here when we use the term “emission altitude,” we mean to refer to a best estimate of the altitude of the peak emission; since the red line layer is broad, we do not intend to suggest a single surface height. The emission altitude is often assumed in literature to be stable within a narrow altitude range, confined within a neutral scale height of a calculable neutral pressure level, or sometimes for convenience simply said to be around ~220–240 km. The generally sound logic behind it is that (a) for dissociative recombination production of $O(^1D)$, it corresponds

to the transition from atomic to molecular constituents where we get the onset of both significant production and significant quenching by collisions with nitrogen molecules; and (b) for auroral particle excitation of $O(^1D)$, the penetration depth of incoming auroral particles is a relatively well-defined energy-dependent stopping height of unity optical depth [e.g., *Rishbeth and Garriott*, 1969], wherein soft electrons (~100 eV) excite $O(^1D)$ where quenching is weak, while that excited by harder electrons is so strongly quenched by collisions with molecular nitrogen that a negligible fraction of $O(^1D)$ lives long enough to emit a 630.0 nm photon before collisional deactivation. In both cases, the altitude of cutoff by quenching is sharp. The quenching by molecular nitrogen (whatever the $O(^1D)$ excitation mechanism) scales as the N_2 density, which varies steeply with altitude having a scale height of around 25 km near these altitudes. These altitudes breathe up and down as the thermosphere expands and contracts over the solar cycle, as well as between quiet and disturbed conditions (most of this variation is often removed by using neutral pressure levels versus kilometers) [e.g., *Rishbeth and Garriott*, 1969]. This is the rationale for the general usage of a peak emission height being estimated within about ±5%.

[3] We address here an important exception to this nominal rule to which attention needs to be drawn in light of recent studies of the cusp, especially under dark dayside conditions. There is a condition when the altitude of greatest emission can double or more, if thermal excitation of $O(^1D)$ becomes strong. It occurs when electrons at energies exceeding 1.96 eV become highly populated by the tail of the bulk

¹SWC, CASS, Physics Department, Utah State University, Logan, Utah, USA.

²Birkeland Centre for Space Science, Department of Physics and Technology, University of Bergen, Bergen, Norway.

³Department of Physics, University of Oslo, Oslo, Norway.

⁴Department of Geophysics, University Centre in Svalbard, Longyearbyen, Norway.

Corresponding author: H. C. Carlson, Center for Atmospheric and Space Sciences, Physics Department, Utah State University, 4405 Old Main Hill, Logan, UT 84322-4405, USA. (herbert.c.carlson@gmail.com)

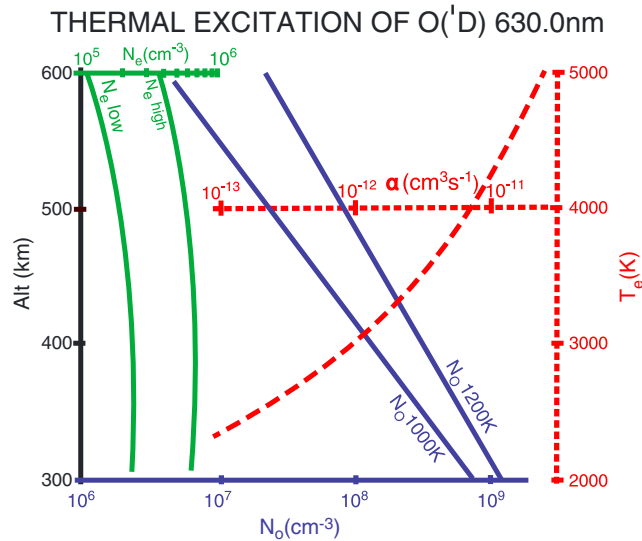


Figure 1. Thermal excitation of O(¹D) 630.0 nm parametric dependence on electron gas temperature T_e , electron density N_e , and atomic oxygen density N_o referenced to a standard model exospheric temperature. $\alpha(T_e)$, the O(¹D) thermal electron excitation rate (cm^3/s), is defined in equation (1) in the text. With N_e , N_o , and $\alpha(T_e)$ all to the same scale for each order of magnitude change, this figure shows that the greatest input parameter sensitivity is to T_e .

electron gas Maxwellian distribution, which could happen once T_e increases much beyond ~ 2500 K. As pointed out by *Lockwood et al.* [1993], a doubling of the emission altitude (4 times the area) could make the difference between a minor and a major role for transient reconnection events in comparison with the more quasi-continuous form.

[4] The exception to which we draw attention here is a consequence of an energy deposition event, triggered in the cusp ionosphere/thermosphere by magnetic reconnection of solar wind at Earth’s magnetopause. These events occur commonly, are transient, and can recur many times per hour on most days in the cusp/midday aurora region.

[5] First, as motivation for this work, we emphasize that events of thermally excited 630.0 nm emissions are significantly more common than generally recognized in the current literature, hence the potential usefulness of the simplified equation and guideline figure to be offered herein. We note that magnetic reconnection, while far from the only mechanism to produce thermally excited emission, is both common for such generation and also one where determination of the emission altitude is especially important. An important motivation for this work is the possible application for estimating the amount of flux entering the polar cap by magnetic reconnection events.

[6] Second, we describe the underlying physics of the thermal excitation mechanism, with emphasis on parameterization in a convenient form to enable quick identification of when thermal electron excitation is likely to be present or not. This parameterized equation and figure should facilitate understanding of the relative sensitivity to dependencies on F region electron density, thermospheric density and exospheric temperature, and most importantly electron gas temperature.

[7] Third, we point out that the incoherent scatter radar technique provides a means to calculate the thermal component of a 630.0 nm emission. The ESR (EISCAT (European

Incoherent Scatter) Svalbard Radar) can measure this (at times dominant) component of aurora regardless of cloud cover. The equations provided here define how the altitude profile of this thermal red line emission is derived from the ESR observations. Figure 1 enables quick estimation of sensitivity to uncertainty in thermospheric model exospheric temperature-density.

[8] Fourth, we illustrate this with two examples of cusp aurora observations, where we show the ESR-derived thermal 630.0 nm component, compare it to the ground-based all-sky imaging photometer (at Ny Ålesund, Svalbard, 1° magnetic north of Longyearbyen) mapping the 630.0 nm arcs, and show that the altitude can only agree when using the ESR T_e -derived altitude (~ 400 – 500 km) versus the conventionally assumed altitude (half that height). Since the two events shown bear the signatures of a magnetic reconnection event [*Carlson et al.*, 2004], this also illustrates cases where the implied magnetic flux entering the polar cap is 4 times higher than that for the commonly assumed height.

[9] Before proceeding, we should briefly distinguish these thermal red line auroras excited by magnetic reconnection events from thermally excited stable auroral red (SAR) arcs which also involve and illuminate understanding of the thermal electron excitation component. SAR arcs are the optical manifestation of the subauroral electron temperature T_e peak. The large body of literature about SAR arcs shows them to be a relatively rare up to hundreds of R red glow in the sky, at subauroral latitudes under highly disturbed ring current conditions, where T_e is elevated to typically >3000 K [e.g., *Kozyra et al.*, 1990, and references therein]. It is thought that ring current energy goes into electrons at high altitudes through a mechanism wherein ring current oxygen ions via Coulomb collisions with plasmaspheric electrons are a significant if not dominant energy source for increasing electron temperatures in the subauroral region. This energy is then

transported downward along plasmapause region field lines to the ionosphere, where cooling by electron-ion collisions brings the electron gas into good thermal contact with the ion gas, which itself is in good thermal contact with the thermosphere. Precipitating electrons of <10 eV energy seen collocated with Dynamics Explorer (DE) satellite transits of SAR arcs suggest that some energy transport is also by a low-energy electron flux. SAR arcs persist for many hours at subauroral latitudes when they (relatively rarely) occur.

[10] Both SAR arcs and any other thermally excited 630.0 nm emission have in common that they are located in areas with significant populations of thermal electrons with energies exceeding 1.96 eV in the high-energy tail of the Maxwellian distribution. These electrons are capable of exciting atomic oxygen to the 1D state during a collision. The unquenched 1D state radiatively relaxes in about 110 s, and its lifetime is shorter when quenched via collisions with molecular nitrogen. Significant 630.0 nm emission only results at altitudes where collisions with molecular nitrogen are infrequent. The intensity of 630.0 nm can be used to observationally define the emission which results from this process. For SAR arcs in the subauroral region, the 630.0 nm intensities are dependent on (1) the electron temperatures, (2) the neutral atmospheric densities of O and N_2 , (3) the f_oF_2 height of the F_2 peak, and (4) the electron density profile.

[11] Important contrasts between SAR arcs and the thermal excitation we address here are (1) rare events versus everyday events, (2) subauroral versus cusp association, (3) stable versus transient, (4) generally excited by hot electrons of Te at ~ 3000 K versus up to 6000 K, and (5) the energy source of SAR arcs tied to ring current oxygen/hydrogen ratios on closed plasmaspheric field lines versus thermal excitation on newly opened flux tubes in the polar cap that experience magnetic curvature forces tracing all the way to the magnetopause.

2. Relevance of Magnetic Reconnection Events

[12] The primary energy deposited into the near-Earth environment by magnetic reconnection events at the magnetopause is dissipation of downgoing Poynting flux into the ionosphere-thermosphere where, by ion frictional drag heating (or equivalently Joule heating as per *Thayer and Semeter* [2004, Appendix A]), the Poynting flux that is not reflected is nearly all passed into the ultimate heat sink, the thermosphere [Carlson, 2012; Carlson *et al.*, 2012]. Strong plasma flow shears have been known to be common in the cusp for a considerable time [e.g., *Pinnock et al.*, 1993, 1995; *Oksavik et al.*, 2004a, 2004b, 2005; *Rinne et al.*, 2007, 2010, 2011; *Moen et al.*, 2008, 2012a, 2012b]. Energy is also deposited by the background cusp particle precipitation, as well as transient injection of electrons and ions precipitating from the newly opened magnetic flux tubes. However, in the presence of strong transient flow shears driven by magnetic reconnection events, energy deposition rates by ion frictional drag heating should dominate the transient particle energy deposition rate [Carlson, 2012, Figure 11; Carlson *et al.*, 2012]. A small fraction of the particle energy goes into the ambient electron gas, heated by the incoming and (mostly) secondary electrons. A very small part of this energy can serve to excite optical emissions that when lost to the thermosphere can act as a valuable tracer

of physical processes in near-Earth space. This work focuses on these tracer optical emissions.

[13] While these tracer optical emissions are our primary focus, we introduce them within the context of magnetic reconnection for three reasons: the association with magnetic reconnection gives important information on frequency of occurrence, timing of occurrence, and location of occurrence. Signatures of magnetic reconnection can be found in the cusp approximately every 5–10 min during southward interplanetary magnetic field (IMF) conditions. These signatures or fingerprints involve a rather precise (within approximately a minute) timing and relative location of five measurable parameters in the ionosphere, two of which are transients in Te and 630.0 nm emission. The relationship between Te and 630.0 nm when/where these signatures are present is what underpins the expectations of when/where to expect Te enhancements, many of which might produce measurable thermally excited high-altitude 630.0 nm emissions. The quantitative equations (1)–(3) herein are what predict when such enhancement actually should occur. Section 5 summarizes these connections.

[14] The connectivity of these five measurable parameters involves tracking energy flow and balance. Mechanical energy in the solar wind, when deflected around Earth's magnetosphere, is converted to electrical energy. This energy carried down magnetic field lines at the Alfvén speed as Poynting flux is then converted back into mechanical energy lost to its ultimate heat sink of the thermosphere. It is useful to view this step in terms of magnetic reconnection at the magnetopause leading to a “magnetic curvature force” sensed in the ionosphere as an $\mathbf{E} \times \mathbf{B}$ force by which ions driven to ~ 1.5 – 3 km/s are frictionally heated in collisions with neutrals in the thermosphere. These plasma flow shears have sharp boundaries (tens of kilometers in space, approximately a minute in time) measurable by the ESR, which can help pinpoint when/where to look for boundaries within which thermally excited 630.0 nm emissions may be found. Details can be found summarized in *Carlson* [2012] and are sketched in section 5 herein.

[15] Complexities of the many processes involved in O (1D) excitation, quenching, and net 630.0 nm emission are beyond the scope of this paper, and the reader is referred to the excellent coverage by *Rees and Roble* [1975]. For focus of auroral red line processes, the reader is referred to *Meier et al.* [1989] for model calculations and *Pallamraju et al.* [2004] for observations. Here we focus only on the thermally excited component of the red line in the cusp, with emphasis on its identification, frequency of occurrence, and better quantification. For energy balance of the electron gas, the cooling rate in the ionosphere is similar that for SAR arcs [e.g., *Kozyra et al.*, 1990]; for energy balance of the ions and thermosphere, including mechanisms more mesoscale than local is important [e.g., *Carlson et al.*, 2012]. Thermal balance of the electron gas has been treated in many places in the literature, mostly under conditions where electron gas cooling in the topside ionosphere is dominated by electron-ion collisions and downward heat conduction (one quantified set of calculations including references even included artificial heating pulses to track transient response times [Mantas *et al.* 1981]). In the case of thermally excited 630.0 nm emissions, the cooling rate to ions alone cannot keep up with the heating rate and Te experiences “runaway”

to the next temperature-limiting process, namely, cooling to collisions with atomic oxygen exciting its $O(^1D)$ state. This further cooling term then becomes the dominant one. A logical follow-on step would be to explore the energy and thermal balance of the overall system.

[16] Auroral electrons of energy ~ 0.1 – 10 keV are readily sensed by their impact excitation (order of kR) of atomic oxygen or molecular species. Harder auroral electron precipitation is commonly tracked in the atomic oxygen 557.7 nm green line and/or molecular nitrogen impact excitation of N_2^+ 391.4 nm or 427.8 nm emission lines. These emissions from deeply penetrating particle fluxes are from relatively well-defined E region altitudes and are not the focus of this paper.

[17] It is common in auroral research to use the 630.0 nm atomic oxygen line to track particle impact signatures of soft auroral electron precipitation [e.g., Sandholt *et al.*, 2002]. It is also common in polar cap (and lower latitude) research to track the motion of relatively high plasma density regions by tracking the 630.0 nm emission excited to $O(^1D)$ in its recombination process [e.g., Lorentzen *et al.*, 2004; Moen *et al.*, 2007]. In both cases, interpretation of angular motion and size of optical features is translated into spatial scales based on an assumed altitude. This is typically taken in the literature to be an ~ 225 – 250 km altitude, valid for the recombination red line emission. We will focus here on the emission altitude of an important category of 630.0 nm optical emissions that are common in the cusp, not due to the steady background of soft cusp particles but transient emission events associated with magnetic reconnection.

[18] Magnetic reconnection events are marked by an optical flash associated with particles dumping out the feet of newly opened flux tubes. The intensity of this “optical flash” exceeds the optical emission due to the particle impact emission from the ongoing background cusp particle precipitation [see, e.g., Carlson *et al.*, 2004, Figure 3]. The magnetic reconnection-driven flash will initially move in the direction of the interplanetary magnetic field (IMF) tension force, with the east-west motion driven by the B_y component which initially exceeds the slower antisunward (southward IMF) component. The antisunward component gives a meridian scanning photometer (MSP) signature matching the morphological definition of a poleward moving auroral form (PMAF). PMAFs have been studied for decades, as summarized by, e.g., Sandholt *et al.* [2002] where many PMAF examples are cataloged by IMF “clock angle” orientation.

[19] Technically, the term PMAF refers to any optical feature with a poleward virtual motion. The PMAF is a morphological descriptor, while magnetic reconnection is a physical process. Not all PMAF signatures need to mark magnetic reconnection, but all magnetic reconnection events must produce a PMAF signature, which depending on brightness may first be detected in contrast against the background cusp emission or later and farther poleward against the background polar cap emission. Magnetic reconnection for southward IMF produces several signatures, all with a very specific sequence in time and location as seen by Carlson *et al.* [2004], including Te, Ti, Vi, Ne, and optical signatures that meet the morphological definition of a PMAF. When initial magnetic reconnection opens a closed magnetic flux tube, the following sequence of events can be detected from

the ground: (1) Soft (hundreds of eV) electron precipitation produces an optical flash at many wavelengths; the 630.0 nm emission delay is shortened by quenching to ~ 30 – 40 s, while the 557.7 nm delay is ~ 0.75 s. (2) The same precipitating soft electrons heat the electron gas Te with a time constant of approximately half a minute near the Ne peak [e.g., Mantas *et al.*, 1981]. (3) With an ~ 2 min delay (Alfvén speed), the plasma begins to move in the direction of magnetic tension. (4) The ion plasma flow speed follows this tension force. (5) With a delay of half a minute [e.g., Skjæveland *et al.*, 2011], the ion gas Ti heats up (frictional drag heating). The poleward boundaries of contours of sharp gradients in Ne, Te, Ti, and 630.0 nm intensity track poleward with these relative time delays, and sharp plasma flow shear boundaries separate background plasma from plasma entrained in these flow shears. The edges of these flow shears are found to seed velocity shear or Kelvin-Helmholtz instabilities [Carlson *et al.*, 2007, 2008], which can also lead to plasma density irregularities and strong radar echoes at decameter HF wavelengths [Moen *et al.*, 2001, 2012a, 2012b; Oksavik *et al.*, 2005, 2011, 2012].

[20] There are many more studies in literature of magnetic reconnection events under southward IMF conditions [see, e.g., Sandholt *et al.*, 2002; Carlson, 2012, and references therein]. Some highlight their occurrence like 20 events in a 4 h period over one midday cusp site as the ESR [Moen *et al.*, 2004; Skjæveland *et al.*, 2011]. It is thus not surprising that this has been called out as a potential means toward the end of estimating how much of the magnetic flux entering the polar cap under southward IMF expansion should be attributed to direct magnetic reconnection. Lockwood *et al.* [1993] applied this approach and found that the analysis would make magnetic reconnection events over the cusp either a minor or a major player, depending on the altitude of the poleward moving 630.0 nm optical features. For a given angular size seen by an all-sky imaging photometer (ASIP), increasing the emission altitude twofold multiplies the area and derived entering flux by four. This square law dependence, along with other derivative properties whose estimate depends on the 630.0 nm emission altitude, is why we must here confront the question of how confidently can we determine the altitude of this emission.

[21] In applying geometric arguments to such data to form estimates of the amount of magnetic flux entering the polar cap, the angular size and motion of these optical signatures give estimates of the physical size and speed of the particle flux boundaries or sharp boundaries in ionospheric plasma density only to the accuracy with which the optical emission altitude is known. Recent observations of the optical and ionospheric plasma signatures characteristic of a series of transient reconnection events at the magnetopause have been published by Carlson *et al.* [2004, 2006] but are often found to show electron gas temperatures of ~ 3000 to 6000 K. The significance of such high temperatures is that this suggests a further source of 630.0 nm emissions, excitation by thermal electrons, for which the emission altitude would be considerably higher. The thermal excitation component can come from about twice the altitude of the electron impact component, which can increase the area by about 4 times and make the difference between reconnection events being a minor or major part of the flux entering the polar cap.

3. Calculated 630.0 nm Optical Emissions

[22] Optical emission altitudes for both ionospheric recombination and particle impact ionization have been well studied in the literature, and here we will simply refer the reader to that work. The altitude parameter dependencies of 630.0 nm emissions for a wide range of altitudes and intensity levels have been studied using incoherent scatter radar data applied to several nights' observation at Arecibo for both stable [Wickwar *et al.*, 1974] and perturbed [Cogger *et al.*, 1974] thermospheric conditions and at higher latitudes [Wickwar and Kofman, 1984; Pallamraju *et al.*, 2004]. The red line recombination component of emission comes from the bottomside of the ionospheric F region peak, where the recombination maximizes, but quenching at the lower altitudes can make the topside contribution important for times of low H_{\max} . The altitude of particle impact-excited optical emissions has been parameterized by Strickland *et al.* [1983] for many optical emissions excited by this precipitation and explicitly for excitation of $O(^1D)$ by Meier *et al.* [1989]. Prompt emission profiles (e.g., 557.7 nm) match excitation profiles well, while 630.0 nm emission profiles depend critically on quenching. The quenching is strong for hard (approximately keV) particles that penetrate to E region heights, decreases proportionally with the molecular nitrogen scale height in the F region, is modest for soft (~ 100 eV) particle excitations, and essentially absent above 300 km.

[23] The third source of 630.0 nm emissions to be considered here is by thermal electron gas excitation. Electrons exceeding 1.96 eV energy can in principle excite the $O(^1D)$ state of atomic oxygen, which upon relaxation emits a 630.0 nm photon. Rees and Roble [1975] have a rather complete description of red line physics and quantify the relationship between heat flux and I-T temperatures, although for their SAR description, the downward heat flux is by conduction from a heat reservoir in closed plasmaspheric flux tubes, while here it is local collisional heating by precipitating soft electrons. Work since [Kozyra *et al.*, 1990] has suggested that soft electron precipitation may contribute to SAR as well. For electron gas temperatures $T_e < 3000$ K, the number of thermal electrons exceeding this threshold leads to negligible emission. For $T_e > 4000$ K, emissions can be many kR. The intensity can be calculated as the line-of-sight integral of the number per unit volume of thermal electrons (Ne) times the number per unit volume of atomic oxygen atoms with which they collide (No) times an electron gas temperature (Te)-dependent coefficient (α).

[24] The excitation cross section $\sigma(E)$ (cm^2), for electron impact excitation of $O(^1D)$, rises very rapidly with electron energy between 1.96 and several eV, and both experimental measurements and theoretical calculations of this energy dependence are extremely difficult. Consequently, determining $\alpha(\text{Te})$, the $O(^1D)$ thermal electron excitation rate (cm^3/s), is the most challenging task in performing such calculations. This is of little issue for electron energies above ~ 10 eV, but the greatest challenge lies just where the greatest Te sensitivity occurs, near 2 eV. Here for $\sigma(E)$, we use Mantas and Carlson [1991, equation 1], as it can be easily integrated over Maxwellian distribution of electrons of temperature Te. They also have published reasons why for aeronomical applications the coefficients of Lan *et al.*, 1972 appear to be most appropriate. Mantas and Carlson [1991, equation 2] further

provide an accurate and user-friendly simple formula for calculating $\alpha(\text{Te})$. Using these formulas, we calculate

$$\alpha(\text{Te}) = 0.15\sqrt{\text{Te}} \frac{(8537 + \text{Te})}{(34,191 + \text{Te})^3} \exp(-22,756/\text{Te}) \quad (\text{cm}^3/\text{s}) \quad (1)$$

so the altitude discriminated (R/km) volume emission rate per kilometer of 630.0 nm emission intensity is

$$\text{thermal } I_{630}(\text{h}) = \alpha(\text{Te}(\text{h}))\text{No}(\text{h})\text{Ne}(\text{h}) \quad (\text{Rayleighs}/\text{km}) \quad (2)$$

and the volume emission rate (Rayleighs) as the line-of-sight integral is

$$\text{thermal } I_{630} = \int_{250 \text{ km}}^{650 \text{ km}} \alpha(\text{Te}(\text{h}))\text{No}(\text{h})\text{Ne}(\text{h})\text{dh} \quad (\text{Rayleighs}) \quad (3)$$

where α is measured in cm^3/s and No(h) and Ne(h) are in cm^{-3} ; while the variables are shown as a function of h which is the altitude in kilometers, the integral must be over the line of sight, and Te is measured in Kelvin.

[25] Figure 1 shows a typical altitude dependence of Ne(h) for high/low plasma density polar cusp conditions, representative values of Mass Spectrometer Incoherent Scatter (MSIS) No(h) for exospheric temperatures of 1000 K and 1200 K, and $\alpha(\text{Te})$ for a typically observed range of Te near the cusp. We find that Ne is the parameter of least impact on the integrated intensity of thermal 630.0 nm emission, and Te clearly dominates. We should repeat the caution in Mantas and Carlson [1991], regarding excitation rate cross sections, that values in the literature are spread by an order of 50%, and Lan *et al.* [1972] was favored as it appeared to be the most complete of those available. The last word on further refinement of absolute cross sections (or absolute 630.0 nm intensity calculations) is likely not in yet, and we will in a future work explore auroral data as an independent test of these coefficients in that regard. Our key point here is separable from that, namely, Te is the dominant variable, its measure can indicate when thermal excitation is negligible or not, and our present knowledge enables good estimates of the altitude of thermal excitation of $O(^1D)$, leading to 630.0 nm emissions.

[26] Figure 1 allows convenient estimates of when thermally excited 630.0 nm emissions are likely to be unimportant or important. In the examples below, we will find that, during transient magnetic reconnection events when regions of corotating subauroral plasma are brought into transpolar flow patterns, Te can be enhanced sufficiently to make thermally excited 630.0 nm of importance. It is when the presence of this effect is most important to estimates of flux entering the polar cap that this altitude correction is at greatest risk of being necessary. We thus proceed to more quantitative calculations for representative cases.

4. Observations

[27] In Figure 2, we show incoherent scatter radar measurements of the electron and ion temperatures T_e and T_i , log Ne, and radar line-of-sight plasma velocity V_i during a type of event that has been found to have signatures of ionospheric patch production in response to a reconnection

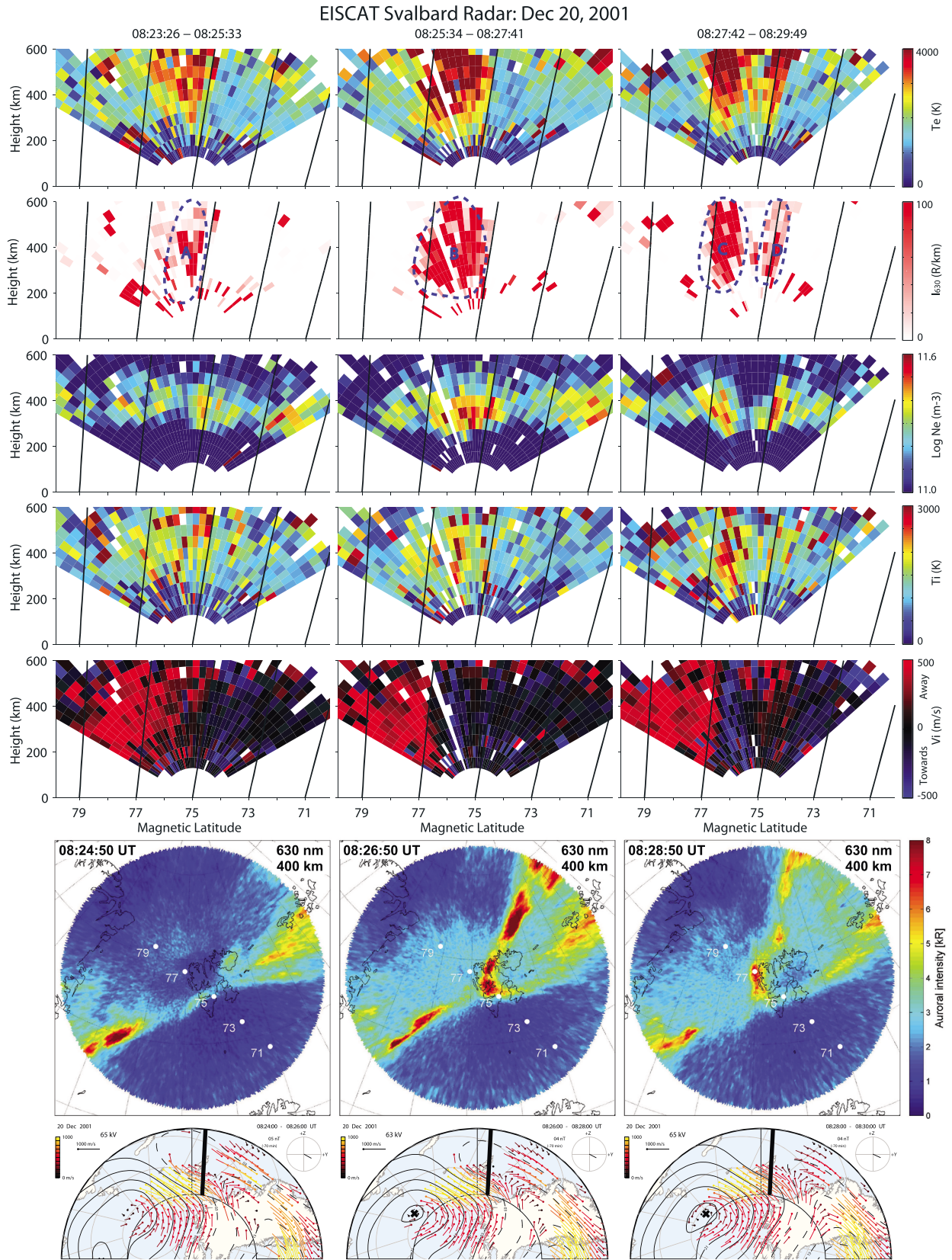


Figure 2

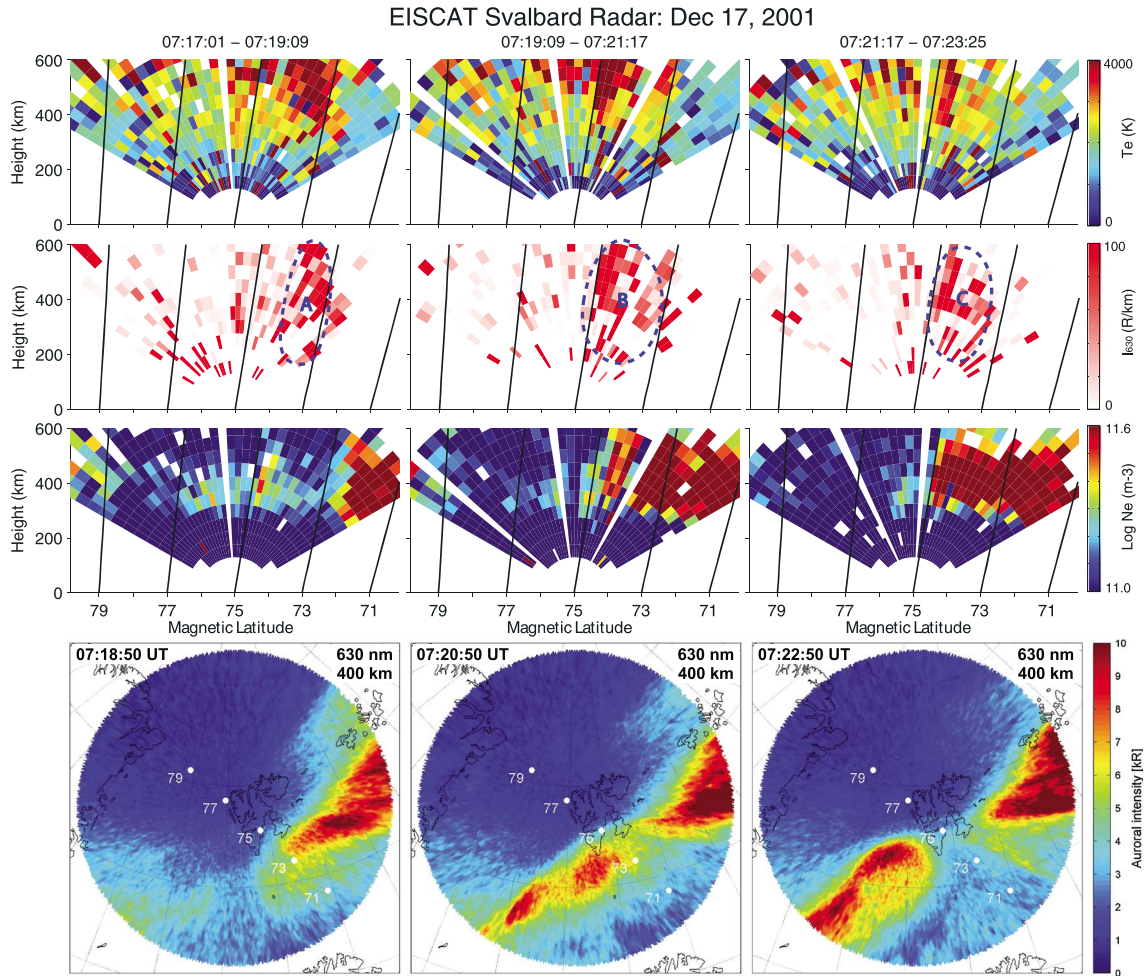


Figure 3. Same as Figure 2 but for 17 December 2001 and condensed to show only the most essential parameters for this study. From top to bottom: measured T_e , derived 630.0 nm volume emission rate R/km , measured N_e , and 630.0 nm all-sky images. Again, the 630.0 nm T_e thermal excited component in ~ 450 km altitude gives the best fit to the observed all-sky image.

event at the magnetopause [Lockwood and Carlson, 1992; Carlson et al., 2004]. The signatures in Figure 2 (previously unpublished data) are almost identical to those seen at 07:55–08:00 UT on 20 January 2001 in a paper published by Carlson et al. [2004, Figure 3] (discussed in paragraphs 7, 10, 16, and 17 therein). Please note that the correct caption for that Figure 3 is “All sky photometric (ASIP) images for the F-region field of view from Nord. The cusp over Svalbard is in the lower right, showing a transient 630.0 nm flash in 1 minute frames, at the reconnection event time (fixed red streak is artifact),” which is misplaced under Figure 4 in the journal (an unfortunate proofreading error by the authors).

[28] Here we call special attention to motion of the T_e boundaries, within the context of both the other parameter boundaries and what we have learned about the physics and morphology of magnetic reconnection signatures. In Figure 2, in the left-hand column showing the 2 min time interval centered on 08:24:30 UT, we see a boundary marked by enhanced T_i and N_e just poleward of 75° magnetic latitude (MLAT) and a change from cool T_e and V_i toward the radar (blue) equatorward of 75° MLAT to hot T_e and V_i away from the radar (red) on the poleward side. Following EISCAT convention, we use blue to specify “Doppler-upshifted toward the radar” and red for plasma flows away from the radar, whichever direction the radar points.

Figure 2. For three successive 2 min time intervals on 20 December 2001, this figure presents seven panels from top to bottom: measured electron gas temperature T_e , derived volume emission rate of 630.0 nm in R/km , measured electron density N_e , measured ion temperature T_i , measured line-of-sight plasma velocity component V_i , an all-sky image of 630.0 nm emissions over Svalbard, and SuperDARN flow patterns for each of these times. The five top rows are all shown on the same scale (0–600 km altitude versus ~ 70 – 80° magnetic latitude), where each independent data point is a 3.2 s integration and the radar scans north-south along the magnetic meridian in a windshield wiper-like sweep of 128 s duration. Most significant for this comparison is the position of the latitude numbers “71, 73, 75, 77, 79” superposed on the all-sky image. The observed brightening in the all-sky data matches the location of the derived thermal volume emission rate.

Thus, red or blue can be east or west, or north or south. For these (and most) data not parallel to B, the horizontal component of V_i well exceeds any vertical. At 08:26:30 UT, the poleward edge of the enhanced Ne has leapt roughly 2° of latitude farther poleward. Two minutes later, the cusp enhanced-Te boundary near 75° MLAT is reappearing, while the new poleward Te-enhanced region is still elevated.

[29] Note particularly that Te (and I_{630}) is weakly elevated within a 1° wide column (75° – 76° MLAT) in the first 2 min (t_1 ~08:24), is high within a 2° wide column (75° – 77° MLAT) in the next 2 min (t_2), and in the last 2 min (t_3) is high at 76° – 77° MLAT and weakly elevated in a 1° wide column centered about 75° MLAT. All enhancements of Te and I_{630} are more sharply defined than a full degree of latitude, and all have edges that are clearly aligned along the magnetic field in the vertical direction. The initial weak Te elevation and I_{630} emission near 75° MLAT is attributed to precipitating cusp electrons. Two minutes later, the strongly enhanced Te and I_{630} emission is attributed to electrons dumping out of the newly opened magnetic flux tube as it moves poleward. Two minutes after that, the still strongly enhanced Te and I_{630} emission near 77° MLAT is attributed to electrons continuing to pour out of the newly opened flux tube, while the weakly enhanced Te and I_{630} emission at 75° MLAT is attributed to the reforming cusp electron boundary which migrates slightly equatorward of its former location prior to entry of the additional flux brought into the equatorward edge of the new polar cap boundary. Consistent with this interpretation is V_i which in the first 2 min (t_1) transitions from corotation (black) to strong away flow (red = away from the radar) at 75° MLAT, in the next 2 min (t_2) shows an initial weak flow shear (red to narrow blue to black), and 2 min later (t_3) exhibits a clear strong wider flow shear reversal (red to blue to black) of strong flow away, strong toward, and corotation equatorward of the cusp. A single spoke of range gates (~ 20 km wide) near 76.7° MLAT at t_3 is black in between the >0.5 km/s away and >0.5 km/s toward flow. Also at t_3 , one sees the onset of away flow as the new cusp equatorward boundary forms. Note that these large-scale flow patterns are the same as seen by Super Dual Auroral Radar Network (SuperDARN) in the bottom strip, where the SuperDARN data have been spatially binned in a 110 km by 110 km grid. Not to ignore any observations, because Ti with a heating time constant of ~ 0.5 min has by t_3 been given at least 2 min to “burn in,” a Ti enhancement must show clearly at t_3 around 76.5° MLAT and be coincident in time and space with the V_i shear observed at t_3 , or else the physics argument here becomes violated. We indeed see the strong Ti enhancement (red versus yellow at $\sim 76.5^\circ$ MLAT) when and where expected for typical reconnection events and even see initial indications of its initial appearance just poleward of 76° MLAT at t_2 . Weakly enhanced Ne equatorward of 73° MLAT is attributed to corotating subcusp ionospheric plasma, in the right location and with low Te and Ti (blue) and corotating V_i (black). Higher-latitude weakly enhanced Ne at t_3 , with $Ne \sim 10^{11.5} m^{-3}$, is consistent with values that are often attributed to production by precipitating cusp particles, as we would do here as well. Note that Ne peak enhancements of $Ne \sim 10^{12} m^{-3}$ would be attributed to transport into the polar cap of upstream solar-produced plasma [e.g., Carlson, 2012]. All observations are therefore entirely consistent with the physics attributed to the data.

[30] In producing the calibrated ASIP images, we optimized the mapping pointing accuracy by matching the background star field in the ASIPs to within a pixel. The color scale sidebar for these images shown in absolute Rayleighs was tuned to bring out key boundaries for comparison to Te boundaries. Note the parallel to B alignment of both Te and the altitude-dependent 630.0 nm intensity calculated (from the observed Te(h), Ne(h), and matched MSIS model No(h)). That so many pixels along so many different ESR beam directions align with B (not the line-of-sight ESR beam direction) speaks very strongly of the data quality for ESR mapping of boundaries. In comparing our observed intensities to those derived from the formula recommended by Mantas and Carlson [1991], equation 3 herein, agreement was within the error bars imposed by our ESR Te-measured values. However, the 3.2 s integration times required to map Ne, Te, Ti, and V_i over an area of ~ 600 km \times 1200 km in ~ 2 min led to error bars on Te and the derived α (Te) matching but are no better than those in the current literature (\sim a factor of 2). Thus, we are now analyzing other data with 60 s integration which in the coming year should give error bars capable of quantitative aeronomy versus mapping boundaries as here.

[31] Figure 3, which is condensed to only the four strips, shows the same features as Figure 2 and is representative of many other events and days. The Te measurements show strong contributions to the height integral of 630.0 nm from altitudes of 300 through 600 km or more. Coincident ground-based 630.0 nm all-sky imager data are in agreement with peak emission altitudes of ~ 400 – 450 km or more and rule out estimates very far from this. It shows the poleward leap of the poleward edge of sunlit high-density Ne described in Lockwood and Carlson [1992], the accompanying poleward leap of other plasma and optical boundaries as in Carlson *et al.* [2006, Figure 1] and described in detail there, and the optical virtual westward motion of the sense as expected from the IMF By control [Moen *et al.* 1999] of polar cap patch entry and implying a faster westward than poleward motion as expected for the large IMF By component at this time. The high Te boundary likewise leaps in lock step with the plasma boundary, as it is indeed plasma on this newly open flux that is heated by the burst of precipitating electrons. The ESR 2 min frame rate exceeds the optical frame rate but tracks in the same way as the 1 min prompt atomic oxygen emission images of Carlson *et al.* [2006, Figure 1] which also shows lock step motion of boundaries of Te, Ti, V_i and Ne, with 777.7 nm boundaries. Note that the lifetime of $O(^1D)$ is ~ 0.5 – 2 min depending on quenching (short at low altitudes, long at high altitude).

5. Discussion

[32] Let us here tie together the several threads in the preceding sections that, in converging, lead to our key points to be made. We have emphasized signatures of magnetic reconnection because one of them is a frequent (up to about 10 per hour [e.g., Moen *et al.*, 2004, Figure 3]) cause of high Te. Associated signatures of reconnection thus not only give information on expected frequency of occurrence but also add much statistics on locating such events in time and space. The burst of electron precipitation out of newly opened magnetic flux tubes must, by collisions, heat the ambient

electron gas they transit. The F region gas temperature heats/cools with a time constant of approximately half a minute [e.g., *Mantas et al.*, 1981]. These commonly observed magnetic reconnection signatures are generally coincident [Carlson, 2012] with commonly observed PMAFs as tracked by meridian scanning photometers MSPs [see, e.g., *Sandholt et al.*, 2002]. Examples are found in *Moen et al.* [2004, Figure 3], *Skjealand et al.* [2011, Figure 2], and other references cited herein.

[33] What has received little attention to date is the impact on T_e and consequences thereof, largely because electrons are of so little mass that T_e can be easily heated by many sources, thereby complicating conclusions from calculations of its thermal balance. In the electron gas thermal balance, the cooling rates are importantly controlled by ionospheric terms, as discussed by, e.g., *Kozyra et al.* [1990] for the physics of SAR arcs. In contrast, the geophysics of the electron gas heating term is importantly different. For stable auroral red arcs, the heat reservoir for T_e heating is large and sluggish and fed by different physics than here. Here the T_e heating source is transient and the heating mechanism more by direct collisions by electrons precipitating from newly opened magnetic flux tubes, rather than downward heat conduction from a reservoir in closed flux tubes. What is simple, once the electron gas is heated to a T_e exceeding ~ 2500 – 3000 K however, the physics in common is that electron gas cooling by conduction and collisions with ions is no longer fast enough and a further T_e cooling term becomes important, namely, thermal electron collisional excitation of the $O(^1D)$ state.

[34] The transiently greater number flux of course enhances the total electron gas heating rate, but most important is that it does so to so great a degree that the cooling processes previously maintaining thermal balance can no longer do so without calling in an additional cooling process. The T_e “runs away” up to that T_e at which the additional cooling process is able to maintain thermal balance. $O(^1D)$ excitation is the new process, which at high-enough T_e introduces an additional cooling cross section, which a new term in the equation has a very different altitude dependence for excitation of $O(^1D)$ and production of 630.0 nm emission. In the usual cusp, suprathermal electrons (order of hundreds of eV) directly excite $O(^1D)$ at their stopping altitude while also heating the electron gas to temperatures held in balance by electron-ion collisions. In the reconnection transient heated cusp, T_e runaway can occur if the electron-ion collisions alone can no longer maintain the electron gas thermal balance, and then with heat conduction playing an important role in heat redistribution along the magnetic field lines, cooling at much higher altitudes by $O(^1D)$ excitation produces the much higher-altitude 630.0 nm emission by collisions with neutral atomic oxygen, rather than simply by thermal electron-ion collisions

[35] This is the intersection toward which many of our earlier points up to here have been heading. What we seek to highlight here are the following: signatures of magnetic reconnection are very common in the southward IMF cusp, PMAFs are likewise, and most coincide for good reasons of physics. Optical flashes at several wavelengths are signatures of enhanced particle dumping; optical flashes at 630.0 nm in principle might include a measurable thermally excited component. Here we make the point that in practice when

T_e exceeds 3500–4000 K, there is a thermal component, and such events should be present most days. With growing effort to add twin optical stations to enable triangulation (rare so far) of cusp emissions, when skies are clear at both sites, 630.0 nm height determination and identification of a red line high-altitude thermal component measurement are perfectly reasonable goals. Also, the ESR T_e measurements can map T_e in time and space including altitude and thus in principle allow an independent measure of the thermally excited 630.0 nm emission component. This should allow much more possible detections from past and future data. We should contrast this with magnetic reconnection events initiated deeper within the polar cap, where for northward IMF, the magnetic tension force can initially be toward the sun, until the magnetic tension force relaxes to let the flux tube motion blend into the general background polar cap flow. Lobe cell reconnection was reported by *Oksavik et al.* [2006]. In situ satellite particle sensors can distinguish initially sunward events versus the cases of initially antisunward motion with in situ ion dispersion measurements [Weiss et al., 1995]. Ions injected from the magnetic merging site at the dayside magnetopause exhibit a time-of-flight ion energy dispersion as they travel to the ionosphere and lag electron flight times.

[36] From the ESR, stand-alone scanning data, or fixed pointing data supported by ASIP or perhaps MSP data, can map boundaries of enhanced T_e . Of the various reasons, this capability is of interest, likely the strongest relates to a question highlighted in the brief closing Futures section of a Cusp review paper by *Smith and Lockwood* [1996] where they note “many questions remain. For example, what is the relative importance of transient reconnection pulses in comparison to the more quasi-continuous form?” This question still remains. *Lockwood et al.* [1993] pointed out that the amount of magnetic flux entering the polar cap during such transient events is proportional to the area of a transient magnetic reconnection event, which if measured by an ASIP as the area of enhanced 630.0 nm emission is proportional to the square of the altitude of emission; they noted that if from an altitude of 250 km, the contribution is minor; if from twice that height, the contribution is major (the steady background cusp emission is at ~ 250 km). They analyzed EISCAT plus coincident ASIP data for two transient reconnection events, concluding an altitude of 250 km for one and finding “evidence that the emission altitude is considerably greater” for the other. They cited that *Wickwar and Kofman* [1984] measured sufficiently high T_e over the cusp at Sondrestromfjord to thermally excite 630.0 nm emission, as supporting evidence for hypothesizing thermal excitation for this latter case, although the high-altitude error bars on T_e measured by EISCAT were too large for direct confirmation of thermal excitation. Surprisingly, very little has been done on this since. The work here should validate the promise of such an undertaking as well as facilitate it.

[37] We have noted the signatures signaling when it is most fruitful to look, pointed out that these events are frequent in the southward IMF cusp, shown that T_e is the most sensitive dependent variable controlling the presence of these events, specified the threshold T_e above which they are likely to be found, and given a user-friendly quantitative formula for estimating the altitude of the thermal component

profile and its intensity from a cusp incoherent scatter radar. We have given the first direct detections of high-altitude 630.0 nm thermally excited red line “flashes,” applying this formula to ESR data and coincident ASIP images. The present scanning data ideal for mapping and tracking boundaries have error bars consistent with but too large to improve upon the presently recommended 630.0 intensity formula. Within the coming year, analysis of existing data with appropriately smaller error bars will be used to provide a formula adequate to go beyond boundary tracking and enable more quantitative aeronomy applications.

6. Summary and Conclusions

[38] We have first given background and motivation for the need for a raised awareness of thermally excited 630.0 nm emissions. One motivation is to use incoherent scatter radar data to calculate and separate thermally excited 630.0 nm emissions from the total, which in auroral regions includes particle precipitation and recombination components. A strong motivation is also the potential for application to the long-standing issue of separating the net contribution of reconnection events to the general cross-polar cap potential drop, such as that treated in considerable detail by *Lockwood et al.* [1993, and references therein]. The question posed by *Smith and Lockwood* [1996] in their section “the future” on important outstanding questions “...what is the relative importance of transient reconnection pulses in comparison to the more quasi-continuous form?” remains to be answered.

[39] We then presented a user-friendly formula for calculating the altitude profile of the thermally excited component of 630.0 nm emissions and the line-of-sight integral of red line 630.0 nm intensity in R, as a function of electron and thermospheric density and temperature. We then summarized this into a parameterized form allowing examination within a single figure of when thermally excited 630.0 nm emission is significant or not. We next took two representative sets of observations of the cusp over Svalbard, using coincident EISCAT Svalbard Radar measurements of plasma properties and coincident 630.0 nm all-sky imaging photometer data, within the context of SuperDARN convection maps. We showed that for events displaying signatures of transient magnetic reconnection, one should expect significant episodes of thermally excited optical emissions, which need to be taken into account for flux transfer estimates. Quantified calculations for these representative case studies demonstrated that the emission altitude derived from the radar data (primarily the observed T_e) matches well with the observed emission altitude (from triangulation). In particular, we mapped the ASIP image onto projections of a series of altitudes in 50 km steps from 150 through 600 km, choosing the altitude at which the 630.0 nm ASIP arc location best aligned with the latitude at which the ESR measured the significantly enhanced T_e . For these data, this approach narrowed collocation to within a ~ 50 km height or $\sim 1/2^\circ$ latitude. This leads to an emission altitude that is more than double of the 225–250 km altitude that conventional estimates would have applied. The underlying physics and known morphology strongly suggest that such heights are representative for events associated with magnetic reconnection signatures. The higher altitude corresponds to

a factor of 4 difference in area based on geometry, which can be enough to change estimates of the magnetic flux entering the polar cap by magnetic reconnection from minor to major [*Lockwood et al.*, 1993]. We hope that the tool we introduce here will enable more quantitative studies to be pursued with both greater ease and confidence. Exploring the physics highlighted in this paper with more sophisticated modeling is also a critical next step.

[40] **Acknowledgments.** Work was sponsored in part by NSF AGS-1011921 and the USTAR Program, SWC, USU. EISCAT is an international association supported by research organizations in Norway (NFR), Sweden (VR), Finland (SA), Japan (NIPR and STEL), China (CRIRP), the United Kingdom (STFC), Germany (DFG, till 2011), and France (CNRS, till 2005). We thank the SuperDARN PIs for provision of the radar data. This project has also been sponsored by the Research Council of Norway, COST action ES0803, and Air Force Office of Scientific Research, Air Force Material Command, USAF, under grant FA8655-10-1-3003.

[41] Robert Lysak thanks Joshua Semeter and another reviewer for their assistance in evaluating this paper.

References

- Carlson, H. C. (2012), Sharpening our thinking about polar cap ionospheric patch morphology, research, and mitigation techniques, *Radio Sci.*, *47*, RS0L21, doi:10.1029/2011RS004946.
- Carlson, H. C., Jr., K. Oksavik, J. Moen, and T. Pedersen (2004), Ionospheric patch formation: Direct measurements of the origin of a polar cap patch, *Geophys. Res. Lett.*, *31*, L08806, doi:10.1029/2003GL018166.
- Carlson, H. C., J. Moen, K. Oksavik, C. P. Nielsen, I. W. McCrea, T. R. Pedersen, and P. Gallop (2006), Direct observations of injection events of subauroral plasma into the polar cap, *Geophys. Res. Lett.*, *33*, L05103, doi:10.1029/2005GL025230.
- Carlson, H. C., T. Pedersen, S. Basu, M. Keskinen, and J. Moen (2007), Case for a new process, not mechanism, for cusp irregularity production, *J. Geophys. Res.*, *112*, A11304, doi:10.1029/2007JA012384.
- Carlson, H. C., K. Oksavik, and J. Moen (2008), On a new process for cusp irregularity production, *Ann. Geophys.*, *26*, 2871–2885.
- Carlson, H. C., T. Spain, A. Aruliah, A. Skjaevland, and J. Moen (2012), First-principles physics of cusp/polar cap thermospheric disturbances, *Geophys. Res. Lett.*, *39*, L19103, doi:10.1029/2012GL053034.
- Cogger, L. L., V. B. Wickwar, and H. C. Carlson (1974), Combined airglow and incoherent scatter observations as a technique for studying neutral atmospheric variations, *Radio Sci.*, *9*(2), 205–210.
- Kozyra, J. U., C. E. Valladares, H. C. Carlson, M. J. Buonsanto, and D. W. Slater (1990), A theoretical study of the seasonal and solar cycle variations of stable aurora red arcs, *J. Geophys. Res.*, *95*(A8), 12,219–12,234.
- Lan, V. K., N. Feautrier, M. Le Doumeuf, and H. Van Regemorter (1972), Cross sections calculations for electron-oxygen scattering using the polarized orbital close coupling theory, *J. Phys. B. Atom. Molec. Phys.*, *5*, 1506–1516.
- Lockwood, M., and H. C. Carlson (1992), Production of polar cap electron density patches by transient magnetopause reconnection, *Geophys. Res. Lett.*, *19*(17), 1731–1734.
- Lockwood, M., H. C. Carlson Jr., and P. E. Sandholt (1993), Implications of the altitude of transient 630-nm dayside auroral emissions, *J. Geophys. Res.*, *98*(A9), 15,571–15,587.
- Lorentzen, D. A., N. Shumilov, and J. Moen (2004), Drifting airglow patches in relation to tail reconnection, *Geophys. Res. Lett.*, *31*, L02806, doi:10.1029/2003GL017785.
- Mantas, G. P., and H. C. Carlson (1991), Reexamination of the $O(^3P \rightarrow ^1D)$ excitation rate by thermal electron impact, *Geophys. Res. Lett.*, *18*(2), 159–162.
- Mantas, G. P., H. C. Carlson, and C. H. Lahoz (1981), Thermal response of the F region ionosphere in artificial modification experiments by HF radio waves, *J. Geophys. Res.*, *86*(A2), 561–574.
- Meier, R. R., D. J. Strickland, J. H. Hecht, and A. B. Christensen (1989), Deducing composition and incident electron spectra from ground based auroral optical measurements: A study of auroral red line processes, *J. Geophys. Res.*, *94*(A10), 13,541–13,552.
- Moen, J., H. C. Carlson, and P. E. Sandholt (1999), Continuous observation of cusp auroral dynamics in response to an IMF B_Y polarity change, *Geophys. Res. Lett.*, *26*(9), 1243–1246.
- Moen, J., H. C. Carlson, S. E. Milan, N. Shumilov, B. Lybekk, P. E. Sandholt, and M. Lester (2001), On the collocation between dayside

- auroral activity and coherent HF radar backscatter, *Ann. Geophys.*, *18*, 1531–1549.
- Moen, J., K. Oksavik, and H. C. Carlson (2004), On the relationship between ion upflow events and cusp auroral transients, *Geophys. Res. Lett.*, *31*, L11808, doi:10.1029/2004GL020129.
- Moen, J., N. Gulbrandsen, D. A. Lorentzen, and H. C. Carlson (2007), On the MLT distribution of *F* region polar cap patches at night, *Geophys. Res. Lett.*, *34*, L14113, doi:10.1029/2007GL029632.
- Moen, J., Y. Rinne, H. C. Carlson, K. Oksavik, R. Fujii, and H. Opgenoorth (2008), On the relationship between thin Birkeland current arcs and reversed flow channels in the winter cusp/cleft ionosphere, *J. Geophys. Res.*, *113*, A09220, doi:10.1029/2008JA013061.
- Moen, J., H. C. Carlson, Y. Rinne, and Å. Skjæveland (2012a), Multi-scale features of solar terrestrial coupling in the cusp ionosphere, *J. Atmos. Sol. Terr. Phys.*, *87–88*, 11–19, doi:10.1016/j.jastp.2011.07.002.
- Moen, J., K. Oksavik, T. Abe, M. Lester, Y. Saito, T. A. Bekkeng, and K. S. Jacobsen (2012b), First in-situ measurements of HF radar echoing targets, *Geophys. Res. Lett.*, *39*, L07104, doi:10.1029/2012GL051407.
- Oksavik, K., J. Moen, and H. C. Carlson (2004a), High-resolution observations of the small-scale flow pattern associated with a poleward moving auroral form in the cusp, *Geophys. Res. Lett.*, *31*, L11807, doi:10.1029/2004GL019838.
- Oksavik, K., F. Soraas, J. Moen, R. Pfaff, J. A. Davies, and M. Lester (2004b), Simultaneous optical, CUTLASS HF radar, and FAST spacecraft observations: Signatures of boundary layer processes in the cusp, *Ann. Geophys.*, *22*, 511–525.
- Oksavik, K., J. Moen, H. C. Carlson, R. A. Greenwald, S. E. Milan, M. Lester, W. F. Denig, and R. J. Barnes (2005), Multi-instrument mapping of the small-scale flow dynamics related to a cusp auroral transient, *Ann. Geophys.*, *23*, 2657–2670.
- Oksavik, K., J. M. Ruohoniemi, R. A. Greenwald, J. B. H. Baker, J. Moen, H. C. Carlson, T. K. Yeoman, and M. Lester (2006), Observations of isolated polar cap patches by the European Incoherent Scatter (EISCAT) Svalbard and Super Dual Auroral Radar Network (SuperDARN) Finland radars, *J. Geophys. Res.*, *111*, A05310, doi:10.1029/2005JA011400.
- Oksavik, K., J. I. Moen, E. H. Rekaa, H. C. Carlson, and M. Lester (2011), Reversed flow events in the cusp ionosphere detected by SuperDARN HF radars, *J. Geophys. Res.*, *116*, A12303, doi:10.1029/2011JA016788.
- Oksavik, K., J. Moen, M. Lester, T. A. Bekkeng, and J. K. Bekkeng (2012), In situ measurements of plasma irregularity growth in the cusp ionosphere, *J. Geophys. Res.*, *117*, A11301, doi:10.1029/2012JA017835.
- Pallamraju, D., S. Chakrabarti, R. Doe, and T. Pedersen (2004), First ground based OI 630 nm optical measurements of daytime cusplike and F-region auroral precipitation, *Geophys. Res. Lett.*, *31*, L08807, doi:10.1029/2003GL019173.
- Pinnock, M., A. S. Rodger, J. R. Dudeney, K. B. Baker, P. T. Newell, R. A. Greenwald, and M. E. Greenspan (1993), Observations of an enhanced convection channel in the cusp ionosphere, *J. Geophys. Res.*, *98*(A3), 3767–3776, doi:10.1029/92JA01382.
- Pinnock, M., A. S. Rodger, J. R. Dudeney, F. Rich, and K. B. Baker (1995), High spatial and temporal resolution observations of the ionospheric cusp, *Ann. Geophys.*, *13*, 919–925.
- Rees, M. H., and R. G. Roble (1975), Observations and theory of the formation of stable auroral red arcs, *Rev. Geophys.*, *13*, 201–242.
- Rinne, Y., J. Moen, K. Oksavik, and H. C. Carlson (2007), Reversed flow events in the winter cusp ionosphere observed by the European Incoherent Scatter (EISCAT) Svalbard radar, *J. Geophys. Res.*, *112*, A10313, doi:10.1029/2007JA012366.
- Rinne, Y., J. Moen, H. C. Carlson, and M. R. Hairston (2010), Stratification of east-west plasma flow channels observed in the ionospheric cusp in response to IMF BY polarity changes, *Geophys. Res. Lett.*, *37*, L13102, doi:10.1029/2010GL043307.
- Rinne, Y., J. Moen, J. B. H. Baker, and H. C. Carlson (2011), Convection surrounding mesoscale ionospheric flow channels, *J. Geophys. Res.*, *116*, A05213, doi:10.1029/2010JA015997.
- Rishbeth, H., and O. K. Garriott (1969), *Introduction to Ionospheric Physics*, Academic Press Inc., New York.
- Sandholt, P. E., H. C. Carlson, and A. Egeland (2002), *Dayside and Polar Cap Aurora*, Kluwer Academic Publishers, Netherlands.
- Skjæveland, Å., J. Moen, and H. C. Carlson (2011), On the relationship between flux transfer events, temperature enhancements, and ion upflow events in the cusp ionosphere, *J. Geophys. Res.*, *116*, A10305, doi:10.1029/2011JA016480.
- Smith, M. F., and M. Lockwood (1996), Earth's magnetospheric cusps, *Rev. Geophys.*, *34*, 233–260.
- Strickland, D. J., J. R. Jasperse, and J. A. Whalen (1983), Dependence of auroral FUV emissions on the incident electron spectrum and neutral atmosphere, *J. Geophys. Res.*, *88*(A10), 8051–8062.
- Thayer, J. P., and J. Semeter (2004), The convergence of magnetospheric energy flux in the polar atmosphere, *J. Atmos. Sol. Terr. Phys.*, *66*, 807–824.
- Weiss, L. A., P. H. Reiff, E. J. Weber, H. C. Carlson, M. Lockwood, and W. K. Peterson (1995), Flow-aligned jets in the magnetospheric cusp: Results from the Geospace Environment Modeling Pilot program, *J. Geophys. Res.*, *100*(A5), 7649–7659.
- Wickwar, V. B., and W. Kofman (1984), Dayside red auroras at very high latitudes: The importance of thermal excitation, *Geophys. Res. Lett.*, *11*(9), 923–926.
- Wickwar, V. B., L. L. Cogger, and H. C. Carlson (1974), The 6300 Å O(¹D) airglow and dissociative recombination, *Planet. Space Sci.*, *22*(5), 709–724.